Korean Journal of Remote Sensing, Vol.22, No.5, 2006, pp.337~350

Neighborhood Correlation Image Analysis for Change Detection Using Different Spatial Resolution Imagery

Jungho Im †

Center for GIS and Remote Sensing, Department of Geography, University of South Carolina, Columbia, SC 29208

Abstract : The characteristics of neighborhood correlation images for change detection were explored at different spatial resolution scales. Bi-temporal QuickBird datasets of Las Vegas, NV were used for the high spatial resolution image analysis, while bi-temporal Landsat TM/ETM+ datasets of Suwon, South Korea were used for the mid spatial resolution analysis. The neighborhood correlation images consisting of three variables (correlation, slope, and intercept) were evaluated and compared between the two scales for change detection. The neighborhood correlation images created using the Landsat datasets resulted in somewhat different patterns from those using the QuickBird high spatial resolution imagery due to several reasons such as the impact of mixed pixels. Then, automated binary change detection was also performed using the single and multiple neighborhood correlation image variables for both spatial resolution image scales.

Key Words : change detection; neighborhood correlation images; automated calibration model; spatial resolution.

1. Introduction

Timely and accurate information on land cover/land use change is essential for effective and efficient management of Earth system processes. Satellite remote sensing has been widely used in land cover/land use change analysis due to spatial synchronization and temporal repeat observation over large geographic regions (Du *et al.*, 2002). There are two types of land cover/land use change detection applications: one to detect the location of change using various change enhancement techniques and the other to extract the type of change (i.e., "from - to" change information) applying classification techniques (Jensen, 2005).

Numerous remote sensing change detection techniques and methods have been developed and evaluated during the past two decades. Traditional remote sensing change detection techniques include image algebra such as vegetation index and change vector analysis (Jensen and Toll, 1982; Michalek *et al.*, 1993; Chavez and Machinnon, 1994; Johnson and Kasischke, 1998), image transformation such as principal component analysis and Chi-square transformation (Collins and Woodcock, 1996; Ridd and Liu, 1998), and post-classification comparison

Received 20 July 2006; Accepted 14 October 2006.

† Corresponding Author: J. Im (ersgis@gmail.com)

(Jensen *et al.*, 1987, 1995). Since it is important to monitor Earth's surface features for environmental and ecosystem analysis, new change detection methods have been constantly proposed. Change detection methods using sophisticated classification algorithms such as decision trees and artificial neural networks (Dai and Khorram 1999; Chan *et al.*, 2001; Im and Jensen, 2005), using fuzzy sets (Metternicht, 2001), and using object-oriented methods (Walter, 2004; Im *et al.*, 2006b) have been also performed. Although a variety of change detection methods have been developed, it should be noted that no single one is best for all change detection investigations. Detailed discussion on various change detection techniques is found in Lu *et al.* (2002) and Jensen (2005).

Im and Jensen (2005) introduced the *Neighborhood Correlation Image Analysis* concept to detect changes in an urban residential area using high spatial resolution remote sensor data. The analysis is based on the fact that local correlation analysis between bi-temporal imagery provides unique change information between two dates. Neighborhood correlation images (NCIs) contain three variables: correlation, slope, and intercept calculated from correlation analysis in a specified neighborhood (e.g., 3×3) between bi-temporal image datasets. Correlation image analysis was extended to the "object" concept using image segmentation (Im *et al.*, 2006b). Since only high spatial resolution imagery (i.e., ADAR 5500, QuickBird) was successfully incorporated in the studies, it is necessary to explore correlation images in other spatial domains (i.e., mid and/or low spatial resolution) and to identify their characteristics in terms of their application to change detection. Thus, bi-temporal QuickBird datasets in high spatial resolution domains (i.e., 0.6×0.6 m) and bi-temporal Landsat TM/ETM$^+$ datasets in mid spatial resolution domains (i.e., 30×30 m) was used to create neighborhood correlation images, and the characteristics of the resultant images were identified and compared. The objectives of this study included 1) the exploration of neighborhood correlation images generated with a 3×3 window at different spatial resolution scales, 2) the identification of impact of spatial resolution on using the neighborhood correlation images for change detection, and 3) the evaluation of binary change detection using the variables of the neighborhood correlation images.

1) Study Area

Two study sites were selected to explore neighborhood correlation images at different spatial resolution scales (Fig. 1). One site (*Site A*) is located around downtown Las Vegas, NV for the high spatial resolution scale, exhibiting new buildings and parking lots developed between two dates. The other site (*Site B*) is Suwon city in South Korea for the middle spatial resolution scale, documenting new urbanized areas including new highways between two different dates. Suwon city is about 118 km^2 and Mt. Guanggyo surrounds the north of Suwon. Agricultural areas still exist on the southwest of Suwon. Suwon has developed since the mid-1980s and its population was up to one million in 2000. Many changes have occurred between the two dates, and particularly many non-urban areas such as field and forest have been urbanized.

2. Methods

1) Remote Sensor Data and Preprocessing

QuickBird imagery from *DigitalGlobe Inc.*, obtained on May 10, 2002 and on May 18, 2003 was used for correlation image analysis of *Site A* in the high spatial resolution domain (i.e., 0.6×0.6 m). Landsat imagery obtained on September 12, 1994

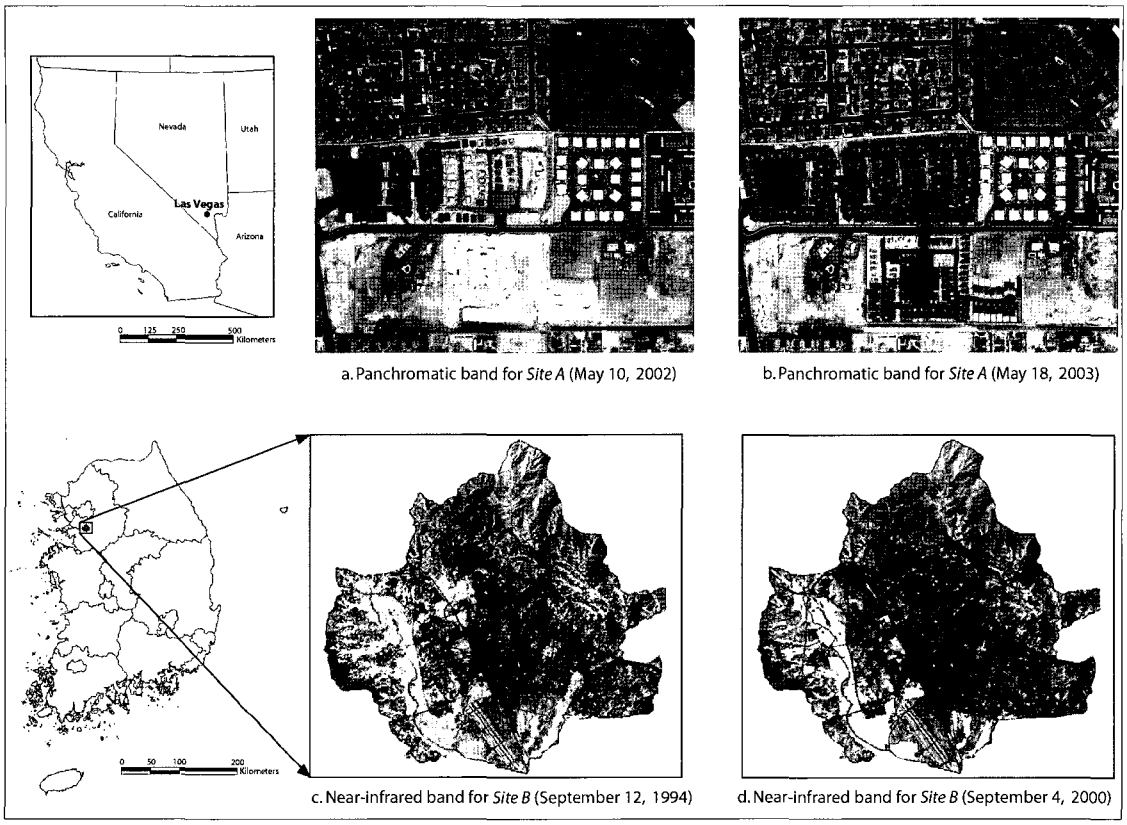

Fig. 1. a), b) Panchromatic bands of bi-temporal QuickBird datasets for *Site A* obtained on May 10, 2002 and May 18, 2003, respectively. c), d) Near-infrared bands of bi-temporal Landsat TM/ETM$^+$ datasets for *Site B* obtained on September 12, 1994 and September 4, 2000, respectively.

(TM) and on September 4, 2000 (ETM$^+$) was used for the middle spatial resolution analysis for *Site B*. The Characteristics of the QuickBird and Landsat data are summarized in Table 1. Panchromatic bands of the QuickBird imagery for *Site A* and near-infrared bands of the Landsat imagery are shown in Fig. 1. Four multispectral bands plus one panchromatic band of the QuickBird datasets and six multispectral bands excluding thermal and panchromatic bands of the Landsat datasets were used in the subsequent analysis.

Although there was a slight difference in the look angles between two QuickBird images (Table 1), orthorectification was not necessary, since no tall buildings existed and the ground was level within the site. The bi-temporal Landsat image datasets were coregistered to a Transverse Mercator (TM) projection using the Tokyo datum while the bi-temporal QuickBird image datasets were coregistered to a Universal Transverse Mercator (UTM) projection in WGS84 with nearest neighbor resampling. Rectification errors in both coregistration were less than 0.5 pixels in RMSE. Although the data acquisition on near-anniversary dates made seasonal variation minimal, radiometric correction of the multi-temporal data was necessary since the correlation image analysis is based on the direct comparison of the pixel values between the bi-temporal imagery (Song *et al.*, 2001). The radiometric normalization method using pseudo invariant features was applied to the bi-temporal QuickBird datasets using six pseudo invariant asphalt and bare soil pixels as radiometric ground control

Table 1. Characteristics of the remotely sensed data for study.

Study area	Acquisition date	Sensor	Image size (pixels)	Spectral bands	Spatial resolution (m)	Radiometric resolution (bits)	Look angle
Site A Las Vegas, NV	May 10, 2002 18:26 GMT	QuickBird	1312 × 1160 (pan)	4 MS 1 Pan	0.6 × 0.6	11	12.8°** 113.8°/76.1°*
	May 18, 2003 18:19 GMT	QuickBird					13.4°** 164.2°/75.2°*
Site B Suwon, South Korea	September 12, 1994	Landsat TM	477 × 467	6 MS (except thermal)	30 × 30	8	
	September 4, 2000	Landsat ETM^+					

* Sensor azimuth / Sensor elevation
** Off-nadir view angle

points. However, due to the difficulty of selecting good radiometric ground control points in the bi-temporal Landsat datasets, the brightness values of each Landsat image dataset were converted into reflectance (Markham and Barker, 1986; NASA, 2006).

2) Reference Data

A total of 400 point samples were randomly generated within *Site A* (i.e., Las Vegas, NV) using a sampling tool developed in ESRI ArcMap 9.1 using Visual Basic (Im, 2006). The change information for each sample location was identified through visual interpretation of the bi-temporal QuickBird datasets and assigned to one of the following seven classes (four unchanged and three change classes): *asphalt, built-up, bare land, vegetation, bare land to asphalt, bare land to built-up*, and *bare land to vegetation* (Table 2).

In order to collect reference data from the bi-temporal Landsat datasets, digital topographic maps with a scale of 1:5,000 and high spatial resolution imagery of Suwon city provided by Google Earth were used as ancillary data. Four hundred (400) point samples were collected within *Site B* (i.e., Suwon, South Korea). The change information for each sample location was assigned to one of the following six classes (four unchanged and two change classes) using the ancillary data: *water, developed, field, forest, field to developed*, and *forest to developed* (Table 2).

3) Correlation Image Analysis

Correlation image analysis is based on spectral *contextual* information created using correlation analysis in a specified neighborhood (or object) between bi-temporal datasets. The contextual information consists of three variables: correlation, slope, and intercept. They contribute to the change detection by providing unique change information. The correlation variable represents Pearson's

Table 2. Reference data information for both study sites.

	Reference data (number of pixels)							
	No change				Change			Total
Site A	*asphalt*	*built-up*	*bare land*	*vegetation*	*bare land to asphalt*	*bare land to built-up*	*bare land to vegetation*	
	64	90	77	52	32	65	20	400
Site B	*water*	*developed*	*field*	*forest*	*field to developed*	*forest to developed*		
	20	115	80	79	83	23		400

product-moment correlation coefficient and the slope and intercept variables are calculated using the least squares estimates. Ideally, if there is no change in a certain location between two dates, the location will have high correlation, a slope around 1, and an intercept around 0. On the other hand, if change has occurred, the correlation values fall off to lower values and the location has variant slope and intercept values. Detailed explanation with regard to correlation image analysis is found in Im and Jensen (2005) and Im *et al.* (2006b).

Based on correlation analysis, *neighborhood correlation images* (NCIs) were generated using the following spatial analysis, which was implemented as a dynamic linked library (DLL) in ESRI ArcMap 9.1 using Visual Basic (Im, 2006):

Correlation image =

$$\frac{N\times K\times\sum_{i=1}^{K}FD1D2_i-(\sum_{i=1}^{K}FD1_i-\sum_{i=1}^{K}FD2_i)}{\sqrt{(N\times K\times\sum_{i=1}^{K}FD12_i-(\sum_{i=1}^{K}FD1_i)^2)\times(N\times K\times\sum_{i=1}^{K}FD22_i-(\sum_{i=1}^{K}FD2_i)^2)}} \quad (1)$$

Slope image =

$$\frac{N\times K\times\sum_{i=1}^{K}FD1D2_i-(\sum_{i=1}^{K}FD1_i\times\sum_{i=1}^{K}FD2_i)}{N\times K\times\sum_{i=1}^{K}FD12_i-(\sum_{i=1}^{K}FD1_i)^2} \quad (2)$$

Intercept image =

$$\frac{\sum_{i=1}^{K}FD2_i-SI\times\sum_{i=1}^{K}FD1_i}{N\times K} \quad (3)$$

where N is the image containing the number of cells in the neighborhood, K is the number of bands in one date of imagery. $FD1_i$ and $FD2_i$ are the images generated applying a focal sum function based on the neighborhood configuration to band i of Date 1 and Date 2 imagery, respectively. $FD1D2_i$ is the image generated applying a focal sum function based on the neighborhood configuration to the image generated by multiplying band i of Date 1 imagery with band i of Date 2 imagery. $FD12_i$ and $FD22_i$ are the images generated applying a focal sum function based on the neighborhood configuration to the images generated by multiplying band i of Date 1 and Date 2 imagery by itself, respectively. SI is the Slope image from Equation 2. Fig. 2 summarizes the data processing flow diagram of creating *neighborhood correlation images* (NCIs). A variety of neighborhood configurations (i.e., type and size) can be applied to correlation image analysis. However, only a 3×3 neighborhood was used to generate the neighborhood correlation images for both sites.

4) Binary Change Detection

The automated calibration model developed in Im *et al.* (2006a) was used for binary change detection based on the 400 reference data for each site. The model was based on a threshold-based approach and the entire burdensome procedure for binary change detection was automated, including calculation of accuracy for each threshold(s), two and/or three dimensional graphs plotting the patterns between the thresholds and accuracies, determination of optimum threshold(s) that yield the highest accuracy, binary change mask generation, and removal of "salt and pepper" noise. Im *et al.* (2006a) points out three advantages of the automated model: 1) the model uses an exhaustive search technique with a stratified sampling design of the search space, which continuously tests threshold(s). 2) Multiple variables can be applied in the model simultaneously, which may yield higher binary change detection accuracy. 3) The model expedites binary change detection processes by automating the burdensome procedures, which saves considerable time and labor. So far, conventional binary change detection based on a calibration method has used a single variable and a threshold due to the computational complexity of multiple variables and thresholds. In addition, a few

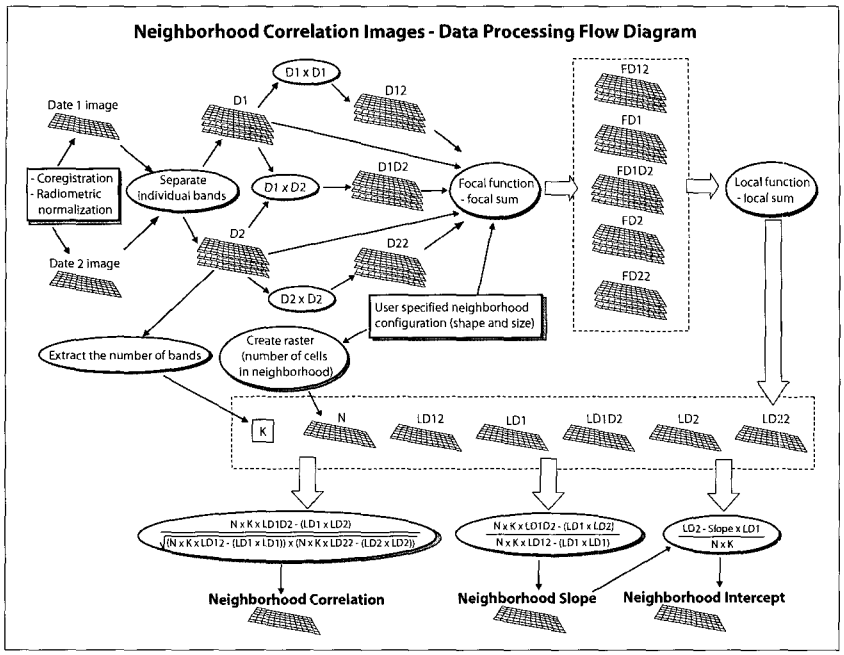

Fig. 2. Data processing flow diagram of *Neighborhood Correlation Images* (NCIs) generation from bi-temporal image datasets.

selected thresholds (e.g., 1, 2, and 3 standard deviations from the mean) have been manually tested in traditional binary change detection approaches. The automated model removed such limitations of traditional binary change detection.

This model requires several inputs, which include image bands (or polygon layers), threshold parameters, and reference data. The input variables (i.e., image bands or polygon layers) can be multiple. Each input variable should be one of three types: *linear, ratio,* and *difference*. One end of the values of a *linear* variable has a high possibility of change, whereas the opposite values indicate no change. Potential change information in a *ratio* variable is symmetrical to a slope of 1, while a *difference* variable has symmetry to an intercept of 0. The type determines conditional expression during calibration. For example, a hypothetical threshold expression of one *ratio* typed variable would be "*if* 0.5 < [variable] < 2, *then* assign no change to a pixel, *else* assign change to the pixel." Threshold range and increment information including *start, step,* and *end* needs to be provided. A point layer is used for reference data and the layer should contain a binary field representing change information (i.e., 0 - no change; 1 - change). More detailed description on the automated binary change detection model is found in Im *et al.* (2006a).

3. Results and Discussion

1) Neighborhood Correlation Images

A 3 × 3 window was used to generate neighborhood correlation images (i.e., correlation, slope, and intercept) for both test sites. The neighborhood correlation images are shown in gray scale in Fig. 3. In the correlation images, the darker pixels (i.e., lower correlation coefficient values) have a greater possibility of change. The darker or the brighter a pixel in the slope and intercept images, the higher the possibility of change the pixel has. Middle gray

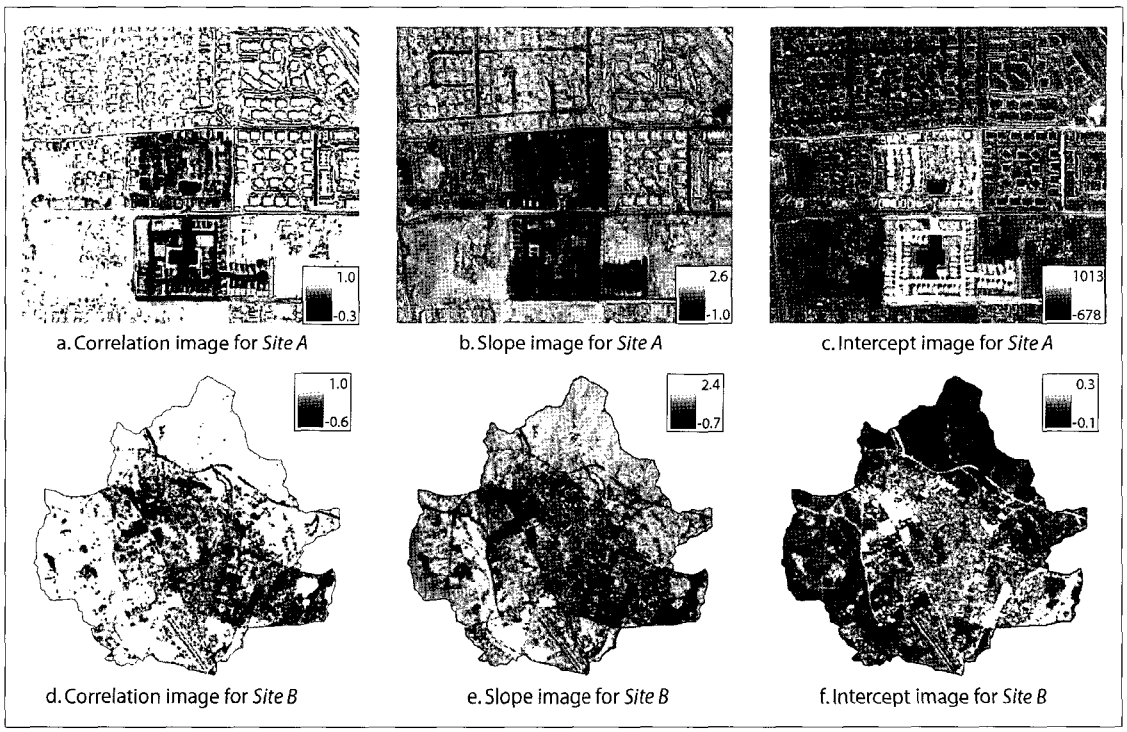

Fig. 3. Neighborhood correlation images (NCIs) generated using a 3 × 3 neighborhood for each site.

colors (slope ~ 1 and intercept ~ 0) correspond to unchanged areas in those two images. Based on visual inspection, the three variables for each site provided somewhat unique change information regardless of spatial resolution.

Fig. 4 depicts three two-dimensional planes based on the 400 reference data for each site: a plane of correlation and slope, a plane of slope and intercept, and a plane of correlation and intercept. Solid symbols represent no change classes in Fig. 4 while open symbols stand for change classes. Four unchanged classes yielded relatively high correlation, with slope values around 1 and intercept values around 0 in the high spatial resolution domain for *Site A* (Figs. 4a, 4c, 4e). The *bare land to asphalt* class resulted in relatively low correlation, lower slope, and higher intercept for *Site A*, which made this class easy to distinguish from the unchanged classes. Some pixels of the *bare land to built-up* class (i.e., new buildings with bright roof tops) yielded high correlation values. Those pixels can be distinguished from the unchanged classes due to their lower slope and higher intercept values (Figs. 4a, 4c, 4e). The *bare land to vegetation* class showed slope values around 1 like the unchanged classes, but it yielded lower correlation and intercept, which made it easy to distinguish the class from the unchanged ones (Figs. 4a, 4c, 4e).

The distribution of the three variables in the lower resolution domain (i.e., *Site B*) showed somewhat different patterns (Figs. 4b, 4d, 4f). Three unchanged classes (i.e., *water*, *field*, and *forest*) resulted in very high correlation values, which made it straightforward to differentiate them from the change classes. However, the *developed* class had correlation values ranging from 0.3 to 0.9. Since the *developed* class also had a relatively wide range of slope and intercept values that overlapped with other

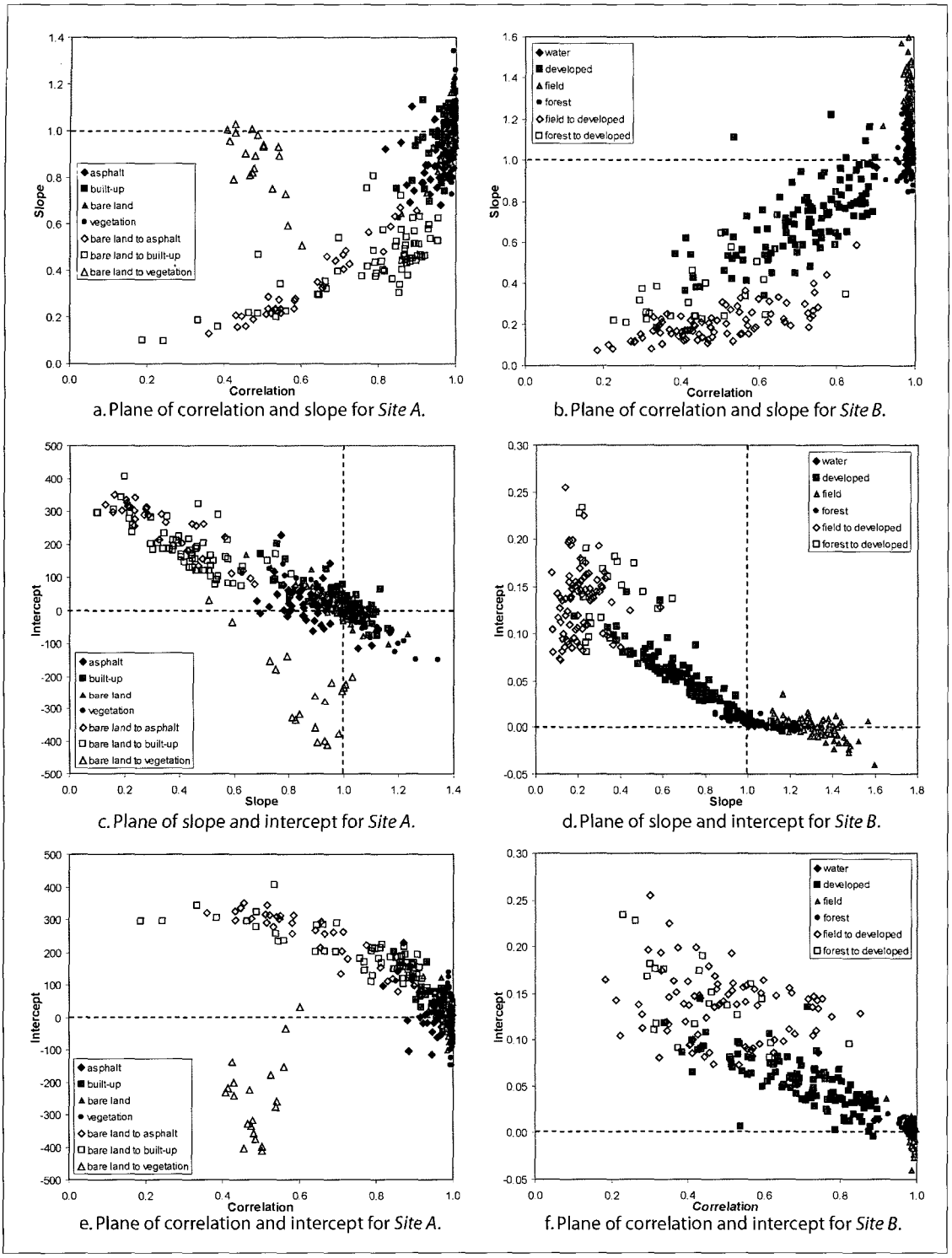

a. Plane of correlation and slope for *Site A*.

b. Plane of correlation and slope for *Site B*.

c. Plane of slope and intercept for *Site A*.

d. Plane of slope and intercept for *Site B*.

e. Plane of correlation and intercept for *Site A*.

f. Plane of correlation and intercept for *Site B*.

Figs. 4. Two-dimensional planes between the three variables (i.e., correlation, slope, and intercept) using the reference data for each site.

unchanged classes, it was hard to distinguish the *developed* pixels from the unchanged ones. It is believed that heterogeneous spectral complexity in the subpixel level of the mid spatial resolution domain results in such variable distribution of the *developed* class. As many pixels in lower resolution imagery such as Landsat data generally combine energy reflected from various materials on the Earth's surface, they, particularly in urbanized area, are often considered as mixed pixels. Some changes in the subpixel level (e.g., traffic, remodeling of buildings, new pavement, etc) might exist in the *developed* class between the two dates. Even though those small changes have actually occurred, they can not be detected in the lower spatial resolution domain such as in 30×30 m Landsat imagery, and such changes are generally disregarded. Consequently, heterogeneity in the mixed pixels of *developed* areas in the lower spatial resolution domain led to low correlation coefficients and variant slope and intercept values in the neighborhood correlation images. The other unchanged classes such as *water*, *field*, and *forest*, which were considered as relatively pure pixels, resulted in very high correlation values. The *field* class yielded relatively high slope and low intercept values. This might be because the *field* class contained large crop area, sensitive to the acquisition date of imagery. The *forest* class resulted in high correlation, but a relatively wide range of slope values, possibly due to the rugged surface of the mountainous area.

As expected, in the two-dimensional planes of slope and intercept (Figs. 4c, 4d), the reference data were distributed along the northwest to southeast direction, which indicated that higher slope usually yielded lower intercept, and vice versa. The two variables were closely interrelated. For example, the change classes (*field to developed, forest to developed*) for *Site B* yielded lower slope (< 1) and higher intercept (> 0).

In summary, many pixels in the site were close to pure pixels in the high spatial resolution domain. These pixels resulted in distinguishable change information in the three neighborhood correlation variables. Some change pixels (e.g., *bare land to built-up*) were confused with the unchanged pixels in one variable (e.g., correlation), but easily identified as change with the other two variables (e.g., slope or intercept). On the other hand, there were relatively fewer pure pixels in the middle spatial resolution domain. Almost all the pixels in the *developed* area were mixed pixels, which showed a somewhat different distribution from the other unchanged classes. Excluding the *developed* class, the change pixels for *Site A* (i.e., high spatial resolution domain) were more obviously identified in the neighborhood correlation images than those for *Site B* (i.e., middle spatial resolution domain). The number of bands used (five versus six) and radiometric resolution (11 bits versus 8 bits) might affect the results.

2) Binary Change Detection

Automated binary change detection was performed using the neighborhood correlation variables and the 400 reference data containing binary change information for each site. Two types of variables were tested: single and multiple. The single variable approach utilized one of the neighborhood correlation, neighborhood slope, and neighborhood intercept for each site. The three variables were used together as a multiple variable group simultaneously for each site.

Graphical calibration results using each single variable for both sites are presented in Fig. 5. Each plot contains three accuracy statistics: Kappa, user's accuracy for change, and producer's accuracy for change. The vertical dashed line represents the optimum threshold resulting in the highest Kappa

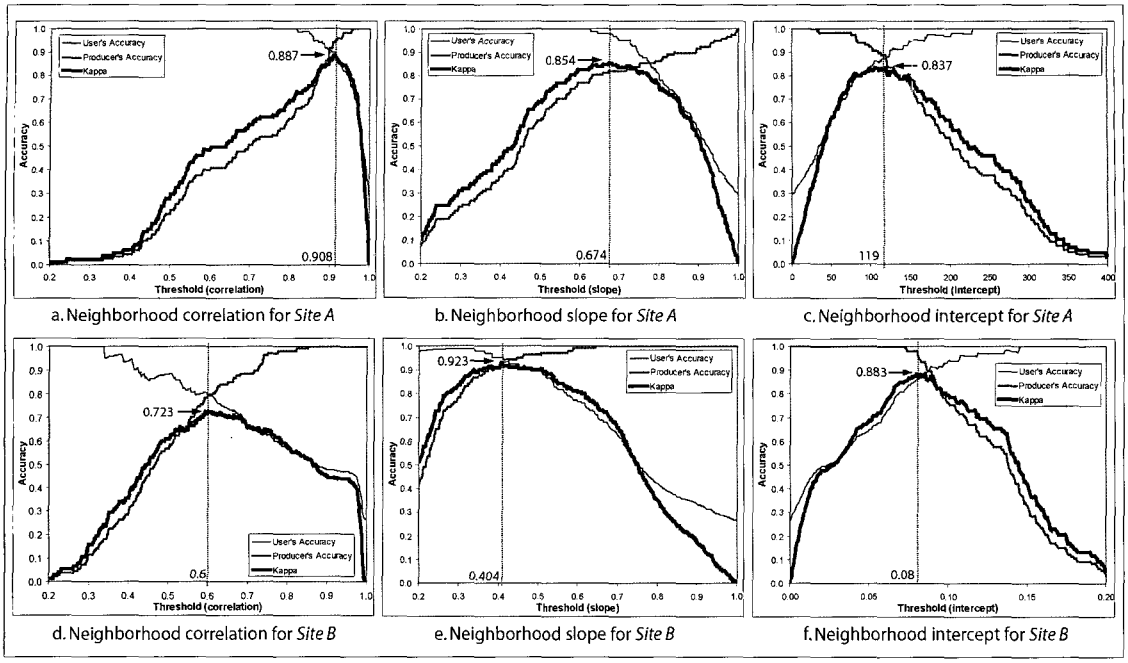

Fig. 5. Automated calibration results using each single variable for both sites. The vertical dotted line represents the optimum threshold yielding the highest Kappa accuracy.

accuracy. The correlation variable resulted in the highest Kappa accuracy (0.887) in the calibrations using the single variables for *Site A*, followed by the slope variable (0.854). In the case of the intercept variable, a high Kappa value of 0.837 was obtained for *Site A* (Fig. 5c). On the contrary, the correlation variable, interestingly, yielded the lowest Kappa accuracy (0.723) among three variables for *Site B*. Instead, the slope variable resulted in the highest Kappa accuracy of 0.923. The mixed pixels, especially in the *developed* class, accounted for this poor performance of the correlation variable in the calibration-based binary change detection in the middle spatial resolution domain. The calibration results using each single variable are summarized in Table 3a.

Calibration results using the multiple variables resulted in better performance than those using the single variable. Fig. 6 depicts the graphical calibration results using the multiple variables for both sites. The multiple variable group for *Site A* resulted in a Kappa of 0.982 and the optimum thresholds for the Kappa were correlation of 0.79, slope of 0.68, and intercept of 250. Thresholds applied to the multiple variables are connected with a series of "AND" functions. Thus, the final threshold-based conditional expression to produce a binary change mask was "*if* [neighborhood correlation] > 0.79 AND 0.68 < [neighborhood slope] < 1.47 AND abs ([neighborhood intercept]) < 250, *then* assign no change to a pixel, *else* assign change to the pixel." The multiple variable group for *Site B* yielded a Kappa of 0.955 with a correlation threshold of 0.3, a slope threshold of 0.38, and an intercept threshold of 0.11. The optimum thresholds and Kappa accuracy with the multiple variables are summarized in Table 3b.

Fig. 7 shows the binary change detection results using the multiple variable group with the optimum thresholds yielding the highest Kappa accuracy for each site. In order to remove "salt-and-pepper" noise in the outputs, the area thresholds of 300 cells (corresponding

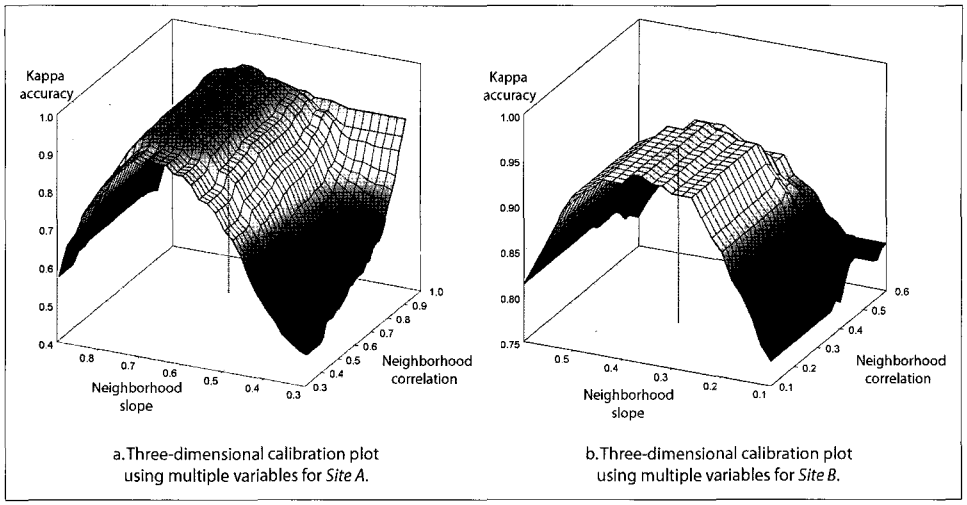

a.Three-dimensional calibration plot using multiple variables for *Site A*.

b.Three-dimensional calibration plot using multiple variables for *Site B*.

Fig. 6. Automated calibration results using the multiple variables for both sites. The vertical dotted line represents the optimum thresholds yielding the highest Kappa accuracy. For display purpose, two variables (i.e., neighborhood correlation and neighborhood slope) are shown while the other variable (i.e., neighborhood intercept) remains constant.

Table 3. Optimum thresholds and Kappa coefficients derived from the calibrations using the single and multiple variables for each study site: a) three single variables and b) multiple variables.

a. Three single variables

Site	Variable	Optimum threshold	Kappa accuracy	Conditional expression for no change
Site A	Neighborhood correlation (nc)	0.908	0.887	0.908 < [nc] < 1
	Neighborhood slope (ns)	0.674	0.854	0.674 < [ns] < 1.484
	Neighborhood intercept (ni)	119	0.837	Abs([ni]) < 119
Site B	Neighborhood correlation (nc)	0.6	0.723	0.6 < [nc] < 1
	Neighborhood slope (ns)	0.404	0.923	0.404 < [ns] < 2.475
	Neighborhood intercept (ni)	0.08	0.883	Abs([ni]) < 0.08

b. Multiple variables

Site	Variables	Optimum threshold	Kappa accuracy	Conditional expression for no change
Site A	Neighborhood correlation (nc)	0.79	0.982	0.79 < [nc] < 1 AND
	Neighborhood slope (ns)	0.68		0.68 < [ns] < 1.47 AND
	Neighborhood intercept (ni)	250		Abs([ni]) < 250
Site B	Neighborhood correlation (nc)	0.3	0.955	0.3 < [nc] < 1 AND
	Neighborhood slope (ns)	0.38		0.38 < [ns] < 2.63 AND
	Neighborhood intercept (ni)	0.11		Abs([ni]) < 0.11

to 108 m^2) and 100 cells (corresponding to 90,000 m^2) were applied to the model for Sites A and B, respectively. Change areas were well detected in both sites based on visual inspection. There was still some "salt-and-pepper" noise in the binary change detection result in the high spatial resolution scale (i.e., *Site A*), especially along the boundaries of the features such as houses. Such noise mostly resulted from the different look angles of the bi-temporal QuickBird datasets. A larger area threshold (e.g., 500 cells) may be applied to the model to remove the noise.

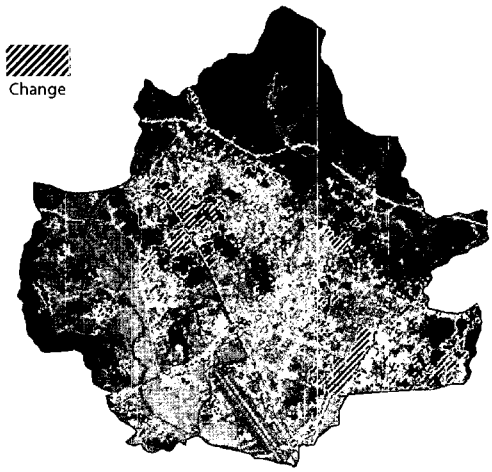

a. Binary change detection result for *Site A* (QuickBird)

b. Binary change detection result for *Site B* (Landsat)

Fig. 7. Binary change detection results using the optimum threshold(s) yielding the highest Kappa accuracy after applying an area threshold of 300 cells for *Site A* and the threshold of 50 cells for *Site B*.

4. Summary and Conclusions

This study explored neighborhood correlation images (NCIs) at two different spatial resolution scales. As we expect, the neighborhood correlation images in the mid spatial resolution scale provided somewhat different patterns from those in the high spatial resolution scale. The characteristics of the neighborhood correlation images in the high resolution domain (i.e., using the QuickBird datasets) include: 1) most of the unchanged pixels yielded high correlation values, but some of the change pixels also resulted in high correlation. Such change pixels were in areas changed from *bare land* to *built-up*, particularly those areas with new houses with bright roof tops. Those pixels generally had lower slope values than the unchanged pixels. 2) Some errors were inevitable along the boundaries of the features within the scene due to the different look angles of the bi-temporal QuickBird datasets. When using high spatial resolution data, acquisition time as well as look angles should be considered in order to minimize shadow and parallax effect. 3) Most unchanged pixels had slope values around 1 and intercept values around 0 in the neighborhood correlation images, while change pixels yielded variant slope and intercept values.

On the other hand, the overall characteristics of the neighborhood correlation images in the middle resolution domain include: 1) homogeneous unchanged areas such as *water* and *forest* yielded very high correlation. However, heterogeneous *developed* areas resulted in variant correlation values ranging from 0.3 to 0.9. This is because the *developed* areas contained a lot of mixed pixels. 2) All change pixels had lower slope and higher intercept values. The fact that the change areas were all from vegetation (i.e., *field*, *forest*), which produced high reflectance in the IR region, explained the pattern.

This study also performed binary change detection using the automated calibration model. The neighborhood correlation image yielded the highest Kappa accuracy (0.887) among three variables for the high spatial resolution domain. However, the neighborhood correlation image variable resulted in the lowest accuracy (a Kappa of 0.723) in the case of

the middle spatial resolution scale due to the variant correlation values in the *developed* areas. Instead, the neighborhood slope variable resulted in a quite good performance (a Kappa of 0.923) in the binary change detection. A neighborhood slope variable might be more critical than a neighborhood correlation variable for change detection. The multiple variables produced the best performance (Kappas of 0.982 and 0.955) in both scales.

This study used one representative pair of dataset for different resolution scale. If other datasets with different features (e.g., number of bands, look angles, radiometric resolution, spectral regions) are used, additional characteristics of neighborhood (or object) correlation images may be identified. Future works will include application of correlation image analysis to other environment such as coastal change or datasets (e.g., hyperspectral, lidar).

References

Chan, J. C., K. Chan, and A. G. Yeh, 2001. Detecting the nature of change in an urban environment: a comparison of machine learning algorithms. *Photogrammetric Engineering & Remote Sensing*, 67(2): 213-225.

Chavez, P. S. JR and D. J. Machinnon, 1994. Automatic detection of vegetation changes in the southwestern United States using remotely sensed images. *Photogrammetric Engineering & Remote Sensing*, 60: 571-583.

Collins, J. B. and C. E. Woodcock, 1996. An assessment of several linear change detection techniques for mapping forest mortality using multitemporal Landsat TM data. *Remote Sensing of Environment*, 56: 66-77.

Dai, X. L. and S. Khorram, 1999. Remotely sensed change detection based on artificial neural networks. *Photogrammetric Engineering & Remote Sensing*, 65(10): 1187-1194.

Du, Y., P. M. Teillet, and J. Cihlar, 2002. Radiometric normalization of multitemporal high-resolution satellite images with quality control for land cover change detection. *Remote Sensing of Environment*, 82: 123-134.

Im, J. and J. R. Jensen, 2005. A change detection model based on neighborhood correlation image analysis and decision tree classification. *Remote Sensing of Environment*, 99: 326-340.

Im, J., J. Rhee, J. R. Jensen, and M. E. Hodgson, 2006a. An automated binary change detection model using a calibration approach. *Remote Sensing of Environment*, in press.

Im, J., J. R. Jensen, and J. A. Tullis, 2006b. Object-based change detection using correlation image analysis and image segmentation. *International Journal of Remote Sensing*, in press.

Im, J., 2006. A Remote Sensing Change Detection System Based on Neighborhood/Object Correlation Image Analysis, Expert Systems, and an Automated Calibration Model, Ph.D. Dissertation, Department of Geography, University of South Carolina.

Jensen, J. R., 2005. Introductory Digital Image Processing: a Remote Sensing Perspective 3rd. Upper Saddle River, NY: Prentice Hall.

Jensen, J. R., E. W. Ramsay, H. E. Mackey, E. J. Christensen, and R. P. Sharitz, 1987. Inland wetland change detection using aircraft MSS data. *Photogrammetric Engineering & Remote Sensing*, 53: 521-529.

Jensen, J. R., K. Rutchey, M. Koch, and S. Narumalani, 1995. Inland wetland change detection in the Everglades Water Conservation Area 2A using a time series of normalized remotely sensed data. *Photogrammetric Engineering & Remote*

Sensing, 61(2): 199-209.

Jensen, J. R. and D. L. Toll, 1982. Detecting residential land use development at the urban fringe. *Photogrammetric Engineering & Remote Sensing*, 48: 629-643.

Johnson, R. D. and E. S. Kasischke, 1998. Change vector analysis: a technique for the multispectral monitoring of land cover and condition. *International Journal of Remote Sensing*, 19(3): 411-426.

Lu, D., P. Mausel, E. Brondizio, and E. Moran, 2004. Change detection techniques. *International Journal of Remote Sensing*, 25(12): 2365-2407.

Markham, B. and J. L. Barker, 1986. Landsat MSS and TM post-calibration dynamic ranges, exoatmospheric reflectances and at-satellite temperatures. *EOSAT Technical Notes*, 1:3-8.

Metternicht, G., 2001. Assessing temporal and spatial change of salinity using fuzzy logic, remote sensing and GIS, foundations of an expert system. *Ecological Modeling*, 144: 163-179.

Michalek, J. L., T. W. Wagner, J. J. Luczkovich, and R. W. Stoffle, 1993. Multispectral change vector analysis for monitoring coastal marine environments. *Photogrammetric Engineering & Remote Sensing*, 59(3): 381-384.

NASA, 2006. Landsat 7 Science Data Users Handbook, Chapter 11 - Data Products. http://ltpwww.gsfc.nasa.gov/IAS/handbook/handbook_htmls/chapter11/chapter11.html.?Last visited June 10, 2006.

Ridd, M. K. and J. Liu, 1998. A comparison of four algorithms for change detection in an urban environment. *Remote Sensing of Environment*, 63: 95-100.

Song, C., C. E. Woodcock, K. C. Seto, M. P. Lenney, and S. A. Macomber, 2001. Classification and change detection using Landsat TM data: when and how to correct atmospheric effects? *Remote Sensing of Environment*, 75: 230-244.

Walter, V., 2004. Object-based classification of remote sensing data for change detection. *ISPRS Journal of Photogrammetry and Remote Sensing*, 58: 225-238.